JACS
JOURNAL OF THE AMERICAN CHEMICAL SOCIETY

Article

pubs.acs.org/JACS

In Situ IR and X-ray High Spatial-Resolution Microspectroscopy Measurements of Multistep Organic Transformation in Flow Microreactor Catalyzed by Au Nanoclusters

Elad Gross,[†] Xing-Zhong Shu,[†] Selim Alayoglu,[†] Hans A. Bechtel,[‡] Michael C. Martin,[‡] F. Dean Toste,*[,†] and Gabor A. Somorjai*[,†]

[†]Department of Chemistry, University of California, Berkeley, California 94720, United States, and Chemical Sciences Division, Lawrence Berkeley National Laboratory, 1 Cyclotron Road, Berkeley, California 94720, United States

[‡]Advanced Light Source, Lawrence Berkeley National Laboratory, 1 Cyclotron Road, Berkeley, California 94720, United States

Supporting Information

ABSTRACT: Analysis of catalytic organic transformations in flow reactors and detection of short-lived intermediates are essential for optimization of these complex reactions. In this study, spectral mapping of a multistep catalytic reaction in a flow microreactor was performed with a spatial resolution of 15 μm, employing micrometer-sized synchrotron-based IR and X-ray beams. Two nanometer sized Au nanoclusters were supported on mesoporous SiO_2, packed in a flow microreactor, and activated toward the cascade reaction of pyran formation. High catalytic conversion and tunable products selectivity were achieved under continuous flow conditions. In situ synchrotron-sourced IR microspectroscopy detected the evolution of the reactant, vinyl ether, into the primary product, allenic aldehyde, which then catalytically transformed into acetal, the secondary product. By tuning the residence time of the reactants in a flow microreactor a detailed analysis of the reaction kinetics was performed. An in situ micrometer X-ray absorption spectroscopy scan along the flow reactor correlated locally enhanced catalytic conversion, as detected by IR microspectroscopy, to areas with high concentration of Au(III), the catalytically active species. These results demonstrate the fundamental understanding of the mechanism of catalytic reactions which can be achieved by the detailed mapping of organic transformations in flow reactors .

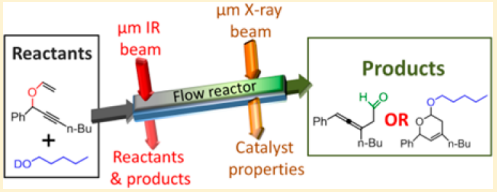

1. INTRODUCTION

Carrying out catalytic transformation in flow reactors instead of batch reactors enhances the sustainability of the catalytic reaction, providing a highly recyclable, scalable, and efficient setup.[1−3] Moreover, the spatial confinement of reactants inside a flow reactor increases the catalytic conversion and enables high control over the residence time of the reactants which can improve product selectivity.[4−7] As a consequence, flow reactors are being widely utilized in the pharmaceutical and chemical industries for the synthesis of complex organic molecules.

The advantages of flow reactors over batch reactors facilitate the substitution of heterogeneous catalysts for their homogeneous counterparts because they can be easily loaded and recycled in flow reactors.[8−11] The heterogenization of homogeneous catalysts is performed by two main approaches. In the first approach, transition metal complexes are grafted on solid supports or directly on the walls of the flow reactor.[12,13] Another, more challenging, approach is to replace the homogeneous catalysts with supported metallic nanoclusters.[5,8,14−19] As part of this effort, we recently reported that small (<2 nm) metallic nanoclusters encapsulated by polypeptides and supported on mesoporous SiO_2 show unique reactivity and selectivity toward a wide range of π-bond activation reactions that were previously solely catalyzed by homogeneous catalysts.[5,14−16,20,21]

Catalytic reactions along flow reactors can be analyzed by a variety of spectroscopic tools, such as fluorescence, IR, Raman, NMR, and X-ray spectroscopy.[22−27] However, these methods usually do not have sufficient spatial or spectral resolution for detailed kinetic analysis of the catalytic reaction.[7] Synchrotron-based spectroscopy can fill this gap with a diffraction-limited IR beam diameter of <10 μm.[28,29] Several initial studies have demonstrated the use of synchrotron IR and X-ray microspectroscopy to characterize simple gas phase catalytic reactions while employing zeolites or metal clusters as catalysts.[24,27,30−35] However, in situ kinetic mapping of complex organic transformation within a flow reactor under reaction conditions has yet to be performed.

In this work, we demonstrate that synchrotron-based microspectroscopy mapping can reveal detailed mechanistic information about catalytic organic transformation. Two nanometer sized Au nanoclusters were loaded on mesoporous SiO_2 support, packed in a flow microreactor, and employed as a catalyst for dihydropyran formation (Scheme 1). The heterogeneous Au catalyst activated this cascade reaction with high yield and selectivity which could not be gained by its homogeneous counterpart. 1D mapping was performed with

Received: December 18, 2013
Published: February 5, 2014

dx.doi.org/10.1021/ja412740p | J. Am. Chem. Soc. 2014, 136, 3624−3629

Scheme 1. Cascade Dihydropyran Synthesis

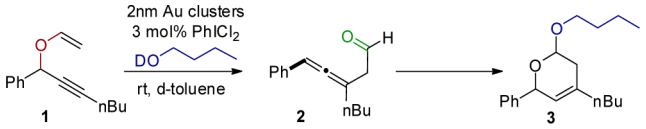

synchrotron-based 10 μm spot-size X-ray and IR beams in order to follow the propagation of the cascade reaction along the flow microreactor with high spatial resolution. We took advantage of the slow evolution of the liquid phase, organic reactants in order to acquire a direct kinetic analysis of products and intermediate formation. The catalytically active species and their distribution along the flow reactor were detected by in situ X-ray absorption microspectroscopy under reaction conditions.

2. EXPERIMENTAL SETUP

Cascade dihydropyran synthesis was chosen as a test reaction for 1D microspectroscopy IR mapping of organic transformation in a flow microreactor. In this reaction, propargyl vinyl ether **1** is catalytically rearranged by the Au catalyst to the primary product allenic aldehyde **2**. Activation of the primary product by the Au catalyst is followed by nucleophilic attack of butanol-d_{10} resulting in the formation of the secondary product, acetal **3**. It was previously shown that the cascade dihydropyran reaction can be catalyzed by homogeneous Au complexes with limited product selectivity.[36]

One of the main advantages in choosing cascade dihydropyran formation as a test reaction for microspectroscopy mapping is that each of the reactants and products show distinguishable IR signatures (Figure 1). As a consequence, the evolution of reactants into products

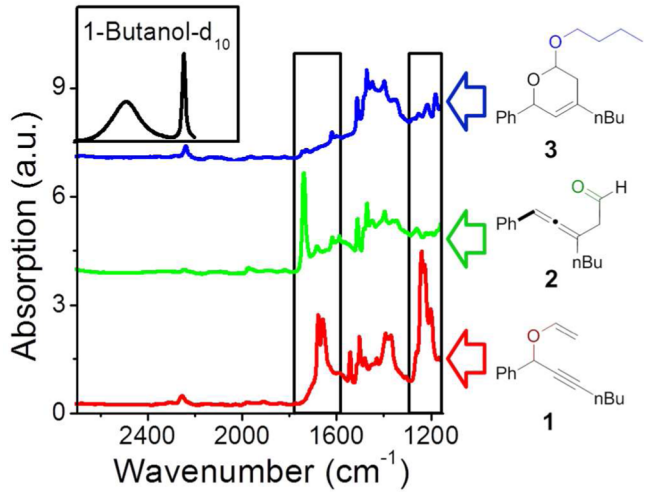

Figure 1. FTIR spectra of the reactant, vinyl ether **1** (red), the primary product, allenic aldehyde **2** (green), and the secondary product, acetal **3** (blue). High-energy regime of IR absorption spectra of butanol-d_{10} (black), the second reactant, is shown as well. The black rectangles mark the areas in which the IR spectra of the different reactants and products can be easily distinguished from each other.

can be precisely monitored by IR spectroscopy. Decrease of the vinyl ether **1** absorption peaks at 1220 and 1650 cm^{-1} indicates the consumption of the reactant, while the formation of the primary product **2** is identified by the CO stretch of the aldehyde at 1720 cm^{-1}. The secondary product **3** is mainly detected by a decrease in the amplitude of the OD stretch of the nucleophilic butanol-d_{10} at 2450 cm^{-1}. The OD bond is consumed by the nucleophilic attack of butanol during the formation of acetal **3**.

Au clusters (2.0 ± 0.3 nm) were synthesized within a fourth-generation polyamidoamine (PAMAM) dendrimer and loaded on SBA-15 (Au@G4OH/SBA-15), a mesoporous SiO_2 support with a surface area of 760 m^2 g^{-1} and a pore diameter of 7 ± 1 nm. The dendrimer-encapsulated Au nanoclusters were easily deposited inside the pores of the mesoporous support, without any modifications in the cluster size.[5] Anchoring of dendrimer-encapsulated Au clusters within the mesoporous support ensured the catalyst's stability under liquid-flow reaction conditions.[15,16] Au@G4OH/SBA-15 catalyst was then packed in a 20 mm long fixed-bed stainless-steel plug flow microreactor with an inner diameter of 0.7 mm. The catalyst was flushed with a solution of 0.02 M of $PhICl_2$, an inorganic oxidizer, in order to oxidize the Au nanoclusters into the catalytically active Au(III) species.[14,16,21] No leaching of metal ions to the solution phase was detected during this step or during the catalytic reaction.

3. RESULTS AND DISCUSSION

3.1. IR Microspectroscopy: Catalytic Yield and Products Selectivity. Samples consisting of 0.5 mmol of vinyl ether **1**, 0.5 mmol of butanol-d_{10}, and 0.05 mmol of $PhICl_2$ were solvated in 10 mL of toluene-d_8 and flowed through the preoxidized Au catalyst at different flow rates at room temperature. As detected by GC and NMR analysis of the products solution, by tuning the residence time of the reactants inside the flow reactor the chemoselectivity of the products can be modified.[5] For example, at a flow rate of 10 mL/h, the short residence time resulted in low conversion (20%) with a primary:secondary (**2**:**3**) products ratio of 5:1. Higher yield (75%) was obtained by decreasing the flow rate by 50-fold to 0.2 mL/h while the selectivity of the products (**2**:**3**) was transformed to 0:100. These results demonstrate the advantage in performing catalytic transformations in flow microreactors. In these systems the chemoselectivity can be widely tuned by the flow rate, enabling isolation of either the primary or secondary product. Tunable selectivity between different products in cascade reactions is not easily achieved while employing homogeneous or heterogeneous catalysts in a batch reactor. Though isolation of the secondary product is possible in batch mode reactions, the exclusive formation of primary product is not a simple task.[4−6]

To analyze the kinetic evolution of products in the flow microreactor the catalyst was deposited in a designated IR cell (the dimensions of the rectangular flow cell were x = 20 mm, y = 3 mm, z = 0.2 mm, a detailed scheme of the IR cell can be found in the Supporting Information, Figure S1). IR absorption spectroscopy measurements were conducted at beamline 1.4.4 of the Advanced Light Source (ALS) at Lawrence Berkeley National Laboratory (LBNL) employing a Thermo Nicolet Nexus 870 and Continuμm XL IR microscope. Line scanning of up to 15 mm was performed along the flow reactor with 15 μm steps, 4 cm^{-1} spectral resolution, and averaging of 256 scans. IR measurements were performed with continuous reactants flow, ensuring that the reactant and product concentrations at each point along the flow reactor were at steady state. IR absorption measurements were conducted as close to the inlet of the flow reactor as possible. Due to physical limitations of the IR flow cell, the initial 40 μm of the flow reactor could not be resolved by IR. As a consequence, the actual zero point of the flow reaction is 40 μm before the beginning of the IR scans.

Subsequent to the flow reaction the products were analyzed by GC. All the conclusions that derive from IR measurements were supported by the GC analysis. The synchrotron-based IR microreactor and the lab-based stainless-steel microreactor were designed to have similar inner volume, ensuring comparable residence time of the reactants. GC analysis

dx.doi.org/10.1021/ja412740p | J. Am. Chem. Soc. 2014, 136, 3624−3629

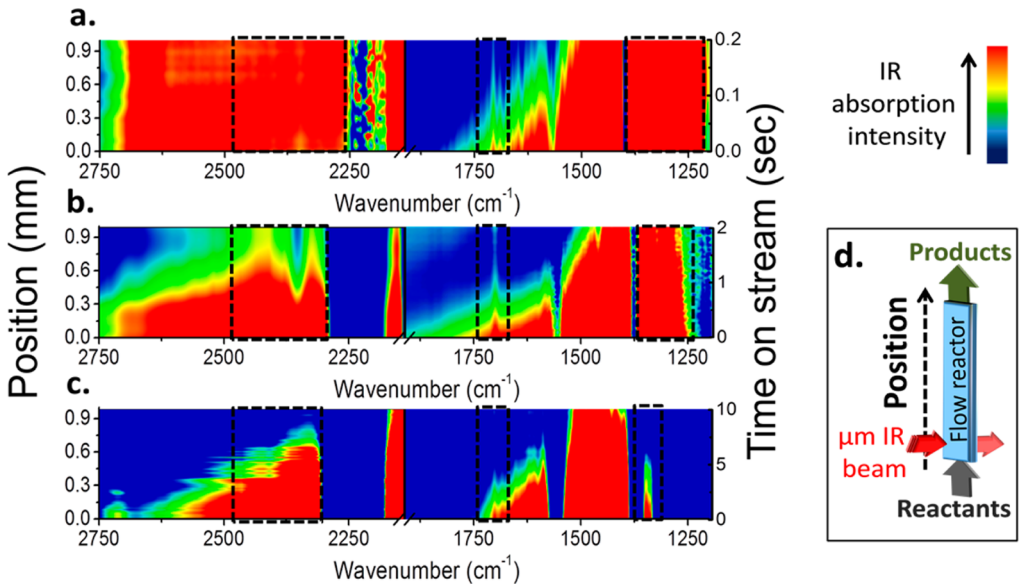

Figure 2. IR absorption microspectroscopy scans along the flow reactor with reactants flow rates of 10 (a), 1 (b), and 0.2 (c) mL/h. Markers were added to direct the eye toward the changes in the IR spectra at different flow rates. A scheme of the micro-IR flow reactor is shown in part d.

verified that the yield and selectivity of the products in these two microreactors were comparable (with variations of up to ±15%).

1D IR absorption spectra mappings were performed along the flow microreactor at three different flow rates (Figure 2a–c). The IR absorption spectra between 2000 and 2150 cm^{-1} were removed due to overabsorption by the toluene-d_8 solvent in this region. IR scans were conducted along the flow reactor, following the reactants into products transformation (Figure 2d).

While employing a high flow rate (10 mL/h) of the reactants solution through the microreactor (Figure 2a) few changes were observed in the lower energy regime (1150–2000 cm^{-1}). A new absorption peak was detected at 1720 cm^{-1}, indicating the formation of the primary product, allenic aldehyde **2**. Interestingly, a maximum in the absorption peak of the primary product was detected at 0.1 mm, before setting into steady absorption amplitude at 0.2 mm. This gradual decrease in aldehyde absorption is correlated to partial catalytic transformation of the primary product into the secondary product, acetal **3**. A minor decrease was obtained in the IR absorption lines which are correlated to vinyl ether **1** (1200–1400 and 1600–1700 cm^{-1}), indicating that a relatively small fraction of the reactant was consumed within this short reactants residence time. Almost no changes were observed in the higher energy range (2150–2750 cm^{-1}), demonstrating negligible consumption of butanol-d_{10} and no IR detectable formation of secondary products under these conditions. These IR measurements indicate that high flow rate conditions resulted in low conversion and mostly the formation of the primary product. These conclusions are supported by the above-mentioned GC and NMR results.

More significant changes in the 1D IR mapping spectra were detected when the residence time of the reactants was increased by an order of magnitude by slowing the flow rate to 1 mL/h (Figure 2b). A decrease in the reactant's, vinyl ether **1**, absorption peaks amplitude (around 1150–1250 cm^{-1}) indicated higher consumption of the reactant, which was followed by a stronger absorption peak of the primary product, aldehyde **2**. After 0.2 mm, a gradual decrease in the aldehyde absorption peak along with a comparable decrease in the higher energy (between 2300 and 2700 cm^{-1}) absorption spectra regime indicated the parallel consumption of butanol-d_{10} and aldehyde **2** to the formation of the secondary product, acetal **3**. It can be concluded that under these flow conditions, longer residence time of the reactants improved the catalytic conversion along with the formation of both the primary **2** and secondary **3** products.

Higher yield was obtained when further increasing the residence time of the reactants by 5-fold with a slower flow rate of 0.2 mL/h (Figure 2c), as obtained by the complete loss of the reactant's absorption peaks at 1150–1250 cm^{-1} after 0.6 mm. Though primary product, **2**, was initially formed with a maximum local IR absorption peak at 0.05 mm, after 0.4 mm the aldehyde IR signature was fully lost. This result indicates the catalytic transformation from primary into secondary product. The formation of the secondary product, acetal **3**, is demonstrated as well by the total consumption of butanol-d_{10} as observed by the gradual decrease of the O–D absorption peak at 2300–2650 cm^{-1} and its disappearance after 0.8 mm. It can be concluded that at this slow flow rate, continuous consumption of vinyl ether **1** was followed by formation of the primary product, allenic aldehyde **2**, which then further reacts with the catalyst and the nucleophile alcohol to form the secondary product, acetal **3**.

Combining GC analysis of the products with IR microspectroscopy mapping indicated that longer residence times of the reactants were followed by an increase in the products yield. Moreover, product selectivity was tuned by changing the residence time of the reactants for the formation of either secondary or primary products.[5]

3.2. Kinetic Analysis of the Cascade Reaction. A detailed kinetic study of the catalytic reaction was performed by integrating the IR absorption peaks of the reactants and products as a function of time on stream and location along the flow reactor. The IR absorption peaks were converted to concentration values (mmol/L) according to GC analysis of the solution before and after the catalytic reaction (Figure 3).

dx.doi.org/10.1021/ja412740p | J. Am. Chem. Soc. 2014, 136, 3624–3629

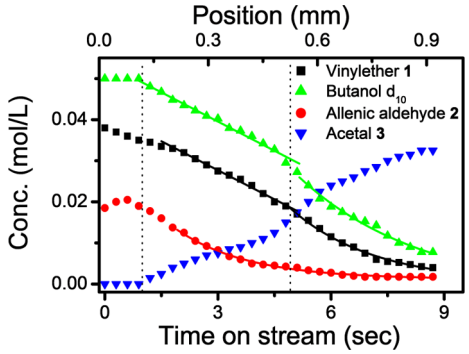

Figure 3. Analysis of distribution of reactants and products as a function of time on stream and location along the flow reactor at a flow rate of 0.2 mL/h. The absorption values of the reactants and products were integrated from the matching IR absorption peak areas and converted to concentration based on GC analysis of the solution. The dotted lines indicate the three different stages of the catalytic reaction.

The kinetic evolution of the reaction at a flow rate of 0.2 mL/h was divided into three stages. During the initial phase of the reaction (0−1.3 s, 0−0.14 mm) the concentration of reactant **1** gradually decreased due to formation of primary product **2**. During this incubation time, no formation of secondary product **3** or consumption of butanol-d_{10} were detected. The early stages of allenic aldehyde **2** formation could not be resolved by IR due to limitations in the detection of the initial 40 μm of the IR microreactor cell.

Through the second part of the reaction (1.3−4.7 s, 0.14−0.52 mm) the two reactants (vinyl ether **1** and butanol-d_{10}) and the primary product (allenic aldehyde **2**) were consumed concurrent with formation of the secondary product, acetal **3**. Zero order kinetics with similar reaction rate coefficient values of −4.2 and −5.0 mM/s were measured for vinyl ether **1** and butanol-d_{10}, respectively. First order kinetics was fitted to the primary product allenic aldehyde **2** with k = 1.9 s^{-1}. At this stage of the reaction the local concentration of the two reactants (vinyl ether **1** and butanol-d_{10}) saturate the catalyst, inducing zero order kinetics. The similarities in the consumption rate of the two reactants are consistent with the fast transformation of primary product (allenic aldehyde **2**) into secondary product (acetal **3**) indicating that the rate-determining step is the conversion of vinyl ether **1** into allenic aldehyde **2**.

At the third phase of the reaction (4.7−9 s, 0.52−1 mm) the concentration of the reactants is low enough to result in the conversion from zero to first order kinetics for the two reactants. The fitted reaction rate coefficient values were 3.1 and 2.2 s^{-1} for vinyl ether **1** and butanol-d_{10}, respectively. At this stage, a continuous low, steady state concentration of allenic aldehyde **2** was detected, demonstrating its pivotal role as an intermediate for the formation of the secondary product, acetal **3**. These results further verified that the rate-determining step in this reaction is the transformation of vinyl ether **1** to allenic aldehyde **2**. This analysis excluded the competitive reaction mechanism that was previously suggested,[36] in which it was proposed that interaction between reactant **1** and butanol can directly lead to the formation of acetal **3**.

Similar kinetic analysis was performed at a higher reactants flow rate of 1 mL/h (Supporting Information, Figure S2). In this case, only the two initial phases of the catalytic reaction were observed. In the first part of the reaction (0−0.5 s, 0−0.3 mm) vinyl ether **1** was consumed in the formation of allenic aldehyde **2**. During the second part of the reaction, a linear decrease (zero order kinetics) in the concentration of the two reactants was measured. The third phase of the reaction was not detected under these flow conditions. A shorter residence time of the reactants resulted in lower catalytic yield and high concentration of the reactants along the flow reactor, which prevented the transformation from zero to first order kinetics.

3.3. X-ray Microspectroscopy: Characterization of Au Catalyst. While the total length of the flow microreactor was 2 cm, the catalytic transformation was completed within the initial 1−2 mm of the reactor. As demonstrated in Figure 4a,

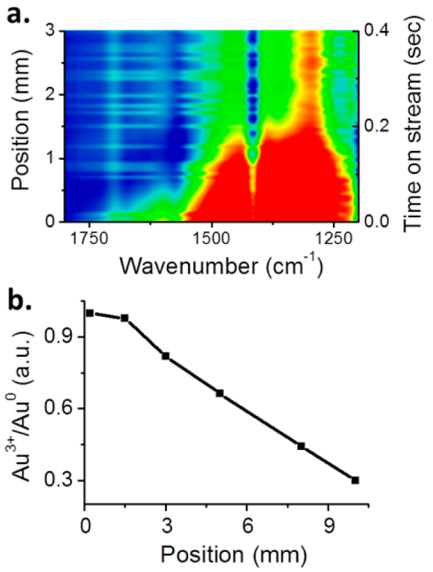

Figure 4. (a) IR microspectroscopy scans along the flow reactor at a flow rate of 5 mL/h. (b) The relative amount of catalytically active Au(III) along the flow reactor as detected by μm-NEXAFS spectroscopy under reaction conditions, with a reactant flow rate of 5 mL/h.

with a reactants flow rate of 5 mL/h, no additional transformation of either the reactant or the primary product was detected after 1.5 mm, although the Au nanoclusters were evenly dispersed all along the reactor. To understand the reason for this localized enhanced catalytic conversion in a specific part of the flow reactor, the oxidation state of the supported catalyst was in situ analyzed by μm-NEXAFS spectroscopy.

X-ray absorption spectroscopy measurements were conducted at beamline 10.3.2 of the ALS at LBNL. The data were collected in fluorescence mode at the Au L_3 edge (11.918 KeV) with a spot size of 16 × 6 μm (details of the experimental flow setup used in these measurements can be found in the Supporting Information, Figure S3). A quartz tube with an inner diameter of 0.96 mm was packed with Au@G4OH/SBA-15 and employed as a flow cell for the NEXAFS experiments. Similar residence times of the reactants in the IR and NEXAFS flow cells (with inner diameters of 0.6 and 0.72 mm^2, respectively) indicate that comparable kinetic rates would be accomplished during the catalytic reaction in these two setups.

The products were analyzed by GC following the catalytic reaction within the X-ray microreactor. The measured products yield and selectivity were similar to those obtained following the catalytic reaction within the IR microreactor. The analysis

dx.doi.org/10.1021/ja412740p | J. Am. Chem. Soc. 2014, 136, 3624−3629

of Au(III)/Au(0) ratio was performed by fitting the acquired spectra, which were measured at different points along the flow reactor, to the reference spectra of Au(III) and Au(0). The measured spectra could not be fitted to the reference Au(I) spectrum, indicating that Au(I) was not a long-lived active species during this reaction (Supporting Information, Figure S4).

NEXAFS measurements along the flow reactor revealed that after 2 mm the concentration of the catalytically active Au(III) species was gradually decreasing due to catalyst reduction to Au(0) (Figure 4b, raw NEXAFS spectra can be found in the Supporting Information, Figure S4). NEXAFS measurements that were conducted following oxidation of Au nanoclusters by $PhICl_2$ and prior to reactants flow, did not detect any major modifications in the concentration of Au(III) along the flow reactor. The reduction of Au(III) to Au(0) can be correlated to the nucleophilic properties of butanol-d_{10}, which can act to some extent as a reducing agent. Butanol-d_{10} can either directly reduce the Au(III) back to its metallic state or attack the oxidizer, $PhICl_2$, decreasing its concentration along the flow reactor. The consequence in both scenarios is similar, the catalyst would be reduced and butanol would be oxidized into butyraldehyde, as indeed was detected in small amounts (~5% of the product) by NMR spectroscopy.

The oxidation of butanol-d_{10} into butyraldehyde-d_8 following the interaction with the oxidized Au catalyst was in situ detected by IR spectroscopy. Butanol-d_{10} (0.25 M) and $PhICl_2$ (5 mM) were flowed at 2 mL/h through the catalyst-packed microreactor. Initial accumulation of butyraldehyde was detected by IR microspectroscopy after 2 mm (Supporting Information, Figure S5). The lower inlet concentration of butanol (0.05 M) employed in the cascade reaction and the slow formation rate of butyraldehyde make it difficult to directly detect the butyraldehyde formation by IR microspectroscopy under conditions employed in the rearrangement reaction.

Interestingly, similar deactivation along the stream of flow reactor was previously reported while employing Rh catalyst for the methane oxidation reaction. In this example, the Rh catalyst was reduced and deactivated by the product molecules which were produced during the reaction along the flow reactor.[27]

3.4. Optimization of the Catalytic Reaction. Based on our spectroscopic analysis we aimed to increase the catalyst stability by reducing its deactivation rate. By decreasing the inlet concentration of the reactants by 5-fold from 0.05 to 0.01 M (at a flow rate of 2 mL/h) the range of the active catalyst along the flow reactor was extended from 2 mm to more than 6 mm, respectively. As a consequence, the catalytic transformation of primary to secondary product was detected up to 6 mm along the flow reactor (Supporting Information, Figure S6). GC analysis of the products indicated that by decreasing the reactants concentration from 0.05 to 0.01 M the primary:secondary (**2**:**3**) products ratio was changed from 3:4 to 1:4 and conversion was increased from 40% to 58%, respectively. These results indicate that by decreasing the inlet concentration of the alcohol, the reduction rate of the active catalyst was decreased, resulting in longer interaction times between the reactants and the catalyst and improved products yield and selectivity.

The NEXAFS and FTIR measurements shown above indicated that with a reactants concentration of 0.05 M the catalytically active Au clusters reside in the initial 10% of the flow reactors volume. According to these results we decreased the amount of catalyst by 10-fold and packed it within the initial 2 mm of the flow reactor. The remaining microreactor volume was packed with pure SiO_2. Following a catalytic reaction with a flow rate of 0.2 mL/h and a concentration of reactants of 0.05 M, the measured yield of the products was 71% with a primary:secondary (**2**:**3**) products ratio of 0:100. Indicating that the residence time of the reactants can be decreased by an order of magnitude from 200 to 20 s without any major changes in the yield and selectivity of products.

4. CONCLUSIONS

We have utilized micrometer-sized synchrotron-sourced IR and X-ray beams for 1D mapping of the organic phase and metallic catalyst during the multistep reaction of dihydropyran formation in a flow microreactor. It was demonstrated that Au@G4OH/SBA-15, a heterogeneous catalyst, activates the cascade reaction with high yield and tunable selectivity, which was gained by adjusting the residence time of reactants in the flow microreactor. The kinetic evolution of the organic transformation and the important role of the primary product as an intermediate were analyzed via in situ IR microspectroscopy with spatial resolution of 15 μm. Direct correlation was obtained between the catalytically active areas along the flow reactor, as detected by IR, to local high concentrations of the catalytically active species, Au(III), as analyzed by μm-NEXAFS spectroscopy. These measurements revealed that the oxidation state of the catalyst and as a consequence its catalytic properties were altered along the flow reactor. As demonstrated in this work, by mapping the gradual evolution of the multistep catalytic process, a better understanding of the mechanism of catalytic reactions and the kinetic role of the intermediates were obtained. These in situ spectroscopy measurements of organic transformation in a flow reactor with high spatial resolution are potentially applicable to numerous catalytic and stoichiometric organic reactions, fulfilling a major challenge in flow chemistry.[7] This novel analysis of catalytic reactions can be directly utilized to probe and improve the catalytic yield and selectivity of organic transformations in flow reactors.

■ ASSOCIATED CONTENT

Supporting Information

Details of the experimental procedure and spectroscopic and microscopic data. This material is available free of charge via the Internet at http://pubs.acs.org.

■ AUTHOR INFORMATION

Corresponding Author

fdtoste@berkeley.edu; somorjai@berkeley.edu

Notes

The authors declare no competing financial interest.

■ ACKNOWLEDGMENTS

We acknowledge support from the Director, Office of Science, Office of Basic Energy Sciences, Division of Chemical Sciences, Geological and Biosciences of the US DOE under contract DE-AC02-05CH11231. The Advanced Light Source is supported by the Director, Office of Science, Office of Basic Energy Sciences, of the U.S. Department of Energy under Contract No. DE-AC02-05CH11231.

REFERENCES

(1) Hartman, R. L.; McMullen, J. P.; Jensen, K. F. *Angew. Chem., Int. Ed.* **2011**, *50*, 7502.
(2) Protasova, L. N.; Bulut, M.; Ormerod, D.; Buekenhoudt, A.; Berton, J.; Stevens, C. V. *Org. Process Res. Dev.* **2013**, *17*, 760.
(3) Newman, S. G.; Jensen, K. F. *Green Chem.* **2013**, *15*, 1456.
(4) Nagaki, A.; Matsuo, C.; Kim, S.; Saito, K.; Miyazaki, A.; Yoshida, J. *Angew. Chem., Int. Ed.* **2012**, *51*, 3245.
(5) Gross, E.; Liu, J. H. C.; Toste, F. D.; Somorjai, G. A. *Nat. Chem.* **2012**, *4*, 947.
(6) Nagaki, A.; Takabayashi, N.; Moriwaki, Y.; Yoshida, J. *Chem.—Eur. J.* **2012**, *18*, 11871.
(7) Elvira, K. S.; Solvas, X. C. I.; Wootton, R. C. R.; deMello, A. J. *Nat. Chem.* **2013**, *5*, 905.
(8) Gross, E.; Krier, J. M.; Heinke, L.; Somorjai, G. A. *Top. Catal.* **2012**, *55*, 13.
(9) Cong, H.; Porco, J. A. *ACS Catal.* **2012**, *2*, 65.
(10) Astruc, D.; Lu, F.; Aranzaes, J. R. *Angew. Chem., Int. Ed.* **2005**, *44*, 7852.
(11) Corma, A.; Garcia, H. *Top. Catal.* **2008**, *48*, 8.
(12) Coperet, C.; Chabanas, M.; Saint-Arroman, R. P.; Basset, J. M. *Angew. Chem., Int. Ed.* **2003**, *42*, 156.
(13) Kobayashi, J.; Mori, Y.; Okamoto, K.; Akiyama, R.; Ueno, M.; Kitamori, T.; Kobayashi, S. *Science* **2004**, *304*, 1305.
(14) Gross, E.; Liu, J. H.; Alayoglu, S.; Marcus, M. A.; Fakra, S. C.; Toste, F. D.; Somorjai, G. A. *J. Am. Chem. Soc.* **2013**, *135*, 3881.
(15) Huang, W. Y.; Liu, J. H. C.; Alayoglu, P.; Li, Y. M.; Witham, C. A.; Tsung, C. K.; Toste, F. D.; Somorjai, G. A. *J. Am. Chem. Soc.* **2010**, *132*, 16771.
(16) Li, Y. M.; Liu, J. H. C.; Witham, C. A.; Huang, W. Y.; Marcus, M. A.; Fakra, S. C.; Alayoglu, P.; Zhu, Z. W.; Thompson, C. M.; Arjun, A.; Lee, K.; Gross, E.; Toste, F. D.; Somorjai, G. A. *J. Am. Chem. Soc.* **2011**, *133*, 13527.
(17) Patil, N. T. *ChemCatChem* **2011**, *3*, 1121.
(18) Sonnenberg, J. F.; Coombs, N.; Dube, P. A.; Morris, R. H. *J. Am. Chem. Soc.* **2012**, *134*, 5893.
(19) Corma, A.; Concepcion, P.; Boronat, M.; Sabater, M. J.; Navas, J.; Yacaman, M. J.; Larios, E.; Posadas, A.; Lopez-Quintela, M. A.; Buceta, D.; Mendoza, E.; Guilera, G.; Mayoral, A. *Nat. Chem.* **2013**, *5*, 775.
(20) Witham, C. A.; Huang, W. Y.; Tsung, C. K.; Kuhn, J. N.; Somorjai, G. A.; Toste, F. D. *Nat. Chem.* **2010**, *2*, 36.
(21) Gross, E.; Somorjai, G. A. *Top. Catal.* **2013**, *56*, 1049.
(22) Xu, B. B.; Zhang, R.; Liu, X. Q.; Wang, H.; Zhang, Y. L.; Jiang, H. B.; Wang, L.; Ma, Z. C.; Ku, J. F.; Xiao, F. S.; Sun, H. B. *Chem. Commun.* **2012**, *48*, 1680.
(23) Buurmans, I. L. C.; Weckhuysen, B. M. *Nat. Chem.* **2012**, *4*, 873.
(24) Stavitski, E.; Weckhuysen, B. M. *Chem. Soc. Rev.* **2010**, *39*, 4615.
(25) Weckhuysen, B. M. *Angew. Chem., Int. Ed.* **2009**, *48*, 4910.
(26) Xu, W. L.; Kong, J. S.; Yeh, Y. T. E.; Chen, P. *Nat. Mater.* **2008**, *7*, 992.
(27) Grunwaldt, J. D.; Hannemann, S.; Schroer, C. G.; Baiker, A. *J. Phys. Chem. B* **2006**, *110*, 8674.
(28) Levenson, E.; Lerch, P.; Martin, M. C. *J. Synchrotron Radiat.* **2008**, *15*, 323.
(29) Nasse, M. J.; Walsh, M. J.; Mattson, E. C.; Reininger, R.; Kajdacsy-Balla, A.; Macias, V.; Bhargava, R.; Hirschmugl, C. J. *Nat. Methods* **2011**, *8*, 413.
(30) Urakawa, A.; Maeda, N.; Baiker, A. *Angew. Chem., Int. Ed.* **2008**, *47*, 9256.
(31) Beale, A. M.; Jacques, S. D. M.; Weckhuysen, B. M. *Chem. Soc. Rev.* **2010**, *39*, 4656.
(32) Stavitski, E.; Kox, M. H. F.; Swart, I.; de Groot, F. M. F.; Weckhuysen, B. M. *Angew. Chem., Int. Ed.* **2008**, *47*, 3543.
(33) Kox, M. H. F.; Domke, K. F.; Day, J. P. R.; Rago, G.; Stavitski, E.; Bonn, M.; Weckhuysen, B. M. *Angew. Chem., Int. Ed.* **2009**, *48*, 8990.
(34) Saida, T.; Sekizawa, O.; Ishiguro, N.; Hoshino, M.; Uesugi, K.; Uruga, T.; Ohkoshi, S.; Yokoyama, T.; Tada, M. *Angew. Chem., Int. Ed.* **2012**, *51*, 10311.
(35) Tada, M.; Ishiguro, N.; Uruga, T.; Tanida, H.; Terada, Y. *Phys. Chem. Chem. Phys.* **2011**, *13*, 14910.
(36) Sherry, B. D.; Maus, L.; Laforteza, B. N.; Toste, F. D. *J. Am. Chem. Soc.* **2006**, *128*, 8132.